

RadVLM: A Multitask Conversational Vision-Language Model for Radiology

Nicolas Deperrois^{1*}, Hidetoshi Matsuo², Samuel Ruipérez-Campillo³, Moritz Vandenhirtz³, Sonia Laguna³, Alain Ryser³, Koji Fujimoto⁴, Mizuho Nishio², Thomas M. Sutter³, Julia E. Vogt³, Jonas Kluckert^{1,5}, Thomas Frauenfelder⁵, Christian Blüthgen⁵, Farhad Nooralahzadeh^{1†}, and Michael Krauthammer^{1†}

¹Department of Quantitative Biomedicine, University of Zurich, Zurich, Switzerland

²Department of Radiology, Kobe University, Kobe, Japan

³Department of Computer Science, ETH Zurich, Zurich, Switzerland

⁴Department of Advanced Imaging in Medical Magnetic Resonance, Kyoto University, Kyoto, Japan

⁵Diagnostic and Interventional Radiology, University Hospital Zurich, Zurich, Switzerland

Abstract

The widespread use of chest X-rays (CXRs), coupled with a shortage of radiologists, has driven growing interest in automated CXR analysis and AI-assisted reporting. While existing vision-language models (VLMs) show promise in specific tasks such as report generation or abnormality detection, they often lack support for interactive diagnostic capabilities. In this work we present RadVLM, a compact, multitask conversational foundation model designed for CXR interpretation. To this end, we curate a large-scale instruction dataset comprising over 1 million image-instruction pairs containing both single-turn tasks – such as report generation, abnormality classification, and visual grounding – and multi-turn, multi-task conversational interactions. After fine-tuning RadVLM on this instruction dataset, we evaluate it across different tasks along with re-implemented baseline VLMs. Our results show that RadVLM achieves state-of-the-art performance in conversational capabilities and visual grounding while remaining competitive in other radiology tasks. Ablation studies further highlight the benefit of joint training across multiple tasks, particularly for scenarios with limited annotated data. Together, these findings highlight the potential of RadVLM as a clinically relevant AI assistant, providing structured CXR interpretation and conversational capabilities to support more effective and accessible diagnostic workflows¹.

1 Introduction

X-rays have played a fundamental role in medicine since their discovery in 1895 (Röntgen, 1895), and continue to be the most frequently used medical imaging modality worldwide due to their convenience and cost-effectiveness (Akhter et al., 2023). Chest X-ray (CXR) remains the most commonly performed radiological exam globally, particularly important for diagnosing and monitoring thoracic conditions such as pneumonia, heart failure, and lung cancer (Çalli et al., 2021). Problematically, the growing volume of CXRs and other imaging studies in recent years have led to a reduction in the time available for radiologists to thoroughly evaluate each case (Peng et al., 2022). As a result, in many countries, the responsibility of interpreting CXRs is often transferred to non-radiology physicians, who typically possess less specialized training and experience. This shift increases the risk of diagnostic errors or misinterpretations (Shammari et al., 2021; Peng et al., 2022).

The shortage of trained personnel for CXR interpretation has led to the exploration of automated agents to assist physicians in diagnostic tasks. In recent years, various deep learning models have shown promise in clinical applications, such as the detection of conditions like COVID-19 pneumonia (Nishio et al., 2020) or pulmonary nodules (Homayounieh et al., 2021). Another extensively studied task is the automated generation of free text reports from CXR images using transformer-based architectures (Nooralahzadeh et al., 2021; Yang et al., 2023; Hyland et al., 2023; Chaves et al., 2024). These models can provide preliminary drafts summarizing key observations from the CXR, offering a potential enhancement to the diagnostic workflow. There is a need to expand the scope of these tools beyond report generation, towards the capability to answer questions about the CXR technique, findings in a region of interest, location of specific abnormalities, and definitions of medical

*Correspondence: nicolas.deperrois@uzh.ch

†Joint senior authorship.

¹Model checkpoints and instruction dataset are publicly available at our project website <https://huggingface.co/KrauthammerLab>

terms. In addition, physicians should be allowed to formulate their queries flexibly and in any order, potentially within a multi-turn, conversational interaction with the assistant (Tu et al., 2024).

Recently, significant advancements in the field of multimodal artificial intelligence (AI) have enabled the development of models such as GPT-4 Vision (GPT4-V, OpenAI, 2024) and Claude (Anthropic, 2024), which have the ability to describe and converse about images with increasing reliability. The training principle behind these models relies on an initial stage to align pretrained vision and language modules, followed by a visual instruction tuning phase where the model learns to respond to image-related queries and commands (Li et al., 2024). Such advancements have inspired the adaptation of multimodal AI assistants for medical applications (Singhal et al., 2023; Li et al., 2023a; Saab et al., 2024).

Despite these advancements, there remains a need for specialized multimodal conversational assistants tailored specifically for CXR interpretation. In this direction, models such as CheXagent (Chen et al., 2024), RaDialog (Pellegrini et al., 2023), or MAIRA-2 (Bannur et al., 2024) were developed, extending beyond report generation to tasks such as observation grounding and visual question answering, covering a larger part of the clinical workflow. However, their capacity to handle diverse and complex user queries, or to respond accurately to multiple prompts within an arbitrary conversational framework, remains limited. Adding these capabilities is critical for comprehensively supporting clinicians’ daily work.

In this study, we build upon state-of-the-art visual instruction-tuning techniques inspired by general-domain applications (Liu et al., 2023; Wang et al., 2024) to construct a compact, multitask conversational foundation model specialized in CXR interpretation. To achieve this aim, we create comprehensive CXR datasets, each featuring diverse modalities including free-text reports, abnormality labels, and visual coordinates, and organize them into a unified instruction dataset. This dataset is comprised of single-turn image-instruction pairs for different tasks and image-conversation pairs designed for more flexible and multi-turn interactions. We then fine-tune a vision-language architecture (Li et al., 2024) on this instruction dataset, naming the resulting model RadVLM, and develop an evaluation pipeline to assess its performance across multiple tasks, systematically comparing it to state-of-the-art generalist and CXR-specific foundation models. Our results show that, despite its relatively compact size, RadVLM achieves competitive performance on individual tasks relevant to clinical practice, providing conversational capabilities within a simple and flexible interface, providing a reliable and user-friendly tool for physicians. Additionally, we compare RadVLM with several existing vision-language models and show that RadVLM matches or outperforms these across both individual and conversational tasks.

In summary, the contributions of this work are as follows:

- We develop a unique instruction dataset that extends beyond report generation to encompass diverse CXR-based tasks, including multi-turn conversational interactions tailored for clinical workflows.
- We design and train RadVLM, a multitask conversational foundation model designed to assist physicians in CXR analysis that solely relies on visual information – avoiding the need for providing additional metadata.
- We employ an evaluation pipeline, re-implementing existing models for comparison and ensuring reproducibility of results.
- We evaluate RadVLM systematically across multiple tasks, demonstrating competitive performance against state-of-the-art vision-language models, both generalist, and medical-specific. In particular, we evaluate conversational abilities in clinical contexts and demonstrate that RadVLM significantly outperforms existing general and clinical VLMs in this aspect.

2 Related works

2.1 Instruction tuning and vision-language models

The advent of autoregressive large language models (LLMs) based on the transformer architecture (Vaswani, 2017) and pre-trained on vast text corpora (Radford et al., 2019; Brown, 2020) has provided the possibility to perform a wide range of language-based downstream tasks. However, the widespread success and accessibility of LLMs, such as ChatGPT, are largely attributed to the instruction-tuning process (Wei et al., 2021; Ouyang et al., 2022). This process commonly involves fine-tuning a pre-trained model on a labeled dataset of diverse instruction-following tasks, ensuring the model can generalize to diverse user instructions in a zero-shot setting.

Instruction-following datasets generally consist of instruction-output pairs and/or multi-turn dialogues (Zheng et al., 2023a) mimicking real-life interaction between users and AI assistants. While early instruction datasets were manually crafted (Wei et al., 2021), a more scalable approach leverages larger LLMs to generate synthetic instruction data (Wang et al., 2022; Peng et al., 2023; Liu et al., 2023), reducing annotation costs.

Beyond the text-only tasks, state-of-the-art proprietary LLMs, such as GPT-4 (Achiam et al., 2023), DeepSeek (Liu et al., 2024; Guo et al., 2025), and Gemini (Team et al., 2023) exhibit advanced vision capabilities, enabling them to process and respond to multimodal instructions. In parallel, open research efforts have led to the development of vision-language models such as LLaVA (Liu et al., 2023) and BLIP-2 (Li et al., 2023b), which introduced effective training strategies for visual instruction tuning. These approaches have inspired the development of vision-language models (VLMs) such as LLaVA-OneVision (Li et al., 2024), Idefics3 (Laurençon et al., 2024), Qwen2-VL (Wang et al., 2024), and Llama-3.2 Vision (Dubey et al., 2024). Similar to text-based LLMs, the instruction-following datasets contain user–assistant Q&A and dialogues, but each example is paired with an image, and the instructions and responses explicitly reflect the image’s content (Feng et al., 2022).

2.2 Vision-language models in radiology

The success of VLMs in the general domain has spurred the development of medical-based VLMs, particularly in domains where image-based interpretation is critical. Proprietary models such as Med-PaLM (Singhal et al., 2023) and Med-Gemini (Saab et al., 2024) have shown remarkable performance across a range of multimodal medical tasks, including medical visual question answering (VQA), report generation, summarization. In parallel, open source models such as LLaVA-Med (Li et al., 2023a) have been developed following similar training strategies as LLaVA (Liu et al., 2023), leveraging biomedical datasets from PubMed (NIH, nd) to design instruction prompts and multi-turn conversations.

Among medical applications, CXR interpretation remains a key area of interest. Early AI-driven models primarily focus on report generation (Nooralahzadeh et al., 2021; Alfarghaly et al., 2021; Tanida et al., 2023; Chaves et al., 2024), supported by the development of clinically relevant evaluation metrics (Jain et al., 2021; Yu et al., 2023a). More recently, research has expanded toward multimodal, multitask CXR assistants capable of integrating multiple functionalities beyond report generation, such as classification, grounding or image generation. Notable examples include CheXagent (Chen et al., 2024) or RoentGen (Bluethgen et al., 2024), though these models lack conversational capabilities.

Other approaches, such as Wolf (Kang et al., 2024), RaDialog (Pellegrini et al., 2023), and M4CXR (Chen et al., 2024), incorporate conversational features but are constrained by predefined response templates, limiting their adaptability in real-world interactions. In this work, we introduce a model that integrates multiple CXR interpretation tasks while enabling flexible, multi-turn dialogue, bridging the gap between task-specific AI models and interactive clinical assistants.

3 Methods

3.1 Instruction dataset

A key step in the development of RadVLM is the construction of an instruction dataset. For this purpose, we first aggregate and process multiple publicly available datasets containing CXR images paired with various attributes, including free-text reports, categorical labels, and bounding boxes. From these sources, we generate a dataset of over 1 million instruction instances, each consisting of a frontal CXR image and a corresponding user–assistant interaction derived from the available attributes. These interactions can be in the form of a single Q&A designed for predefined tasks (single instructions) or of a multi-turn exchange (conversations). The composition of this instruction dataset is detailed below and summarized in Table 1.

3.1.1 Free-text report generation

In alignment with existing CXR models, we aim to generate clinically coherent radiology reports from CXR images. To achieve this, we collect public datasets containing CXRs paired with anonymized free-text reports. Radiology reports often compare to and refer to prior X-ray examinations when discussing current radiological findings. These earlier images should be provided as part of the prompt when conducting report generation based on raw radiology reports (Kim et al., 2023; Bannur et al., 2024). As we here focus on the analysis of a single CXR image, we use GPT4o-mini to remove mentions of prior studies, in line with recent work on report generation (Chen et al., 2024; Chaves et al., 2024).

We leverage two public datasets for the report generation task:

MIMIC-CXR (Johnson et al., 2019), which contains 377,110 CXR images paired with free-text radiology reports describing findings and patient history. After filtering, we retain 232,344 image-text pairs in the training set and 3,282 in the test set.

CheXpert-Plus (Chambon et al., 2024), which features 223,228 image-report pairs from 187,711 studies. Applying the same filtering process as for MIMIC-CXR results in a dataset of 178,368 image-text pairs.

a. Report generation



Draft a concise report for this image.



Small right pleural effusion is present. Minimal right lower lobe atelectasis is likely. The right lung is otherwise clear. No appreciable pneumothorax is seen. Biapical margin thickening, left worse than right, is seen. The left lung is well-expanded and clear. The heart size is normal. Hemi arthroplasty is seen on the right shoulder.

b. Abnormality classification



Are there identifiable abnormalities on this Chest X-ray?

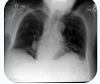


Yes, there is one abnormality identified: pneumothorax.

c. Visual grounding: Anatomy/Abnormality



Indicate the position of the *left apical zone*.



The left apical zone is situated at [0.57, 0.14, 0.85, 0.3] in the image.



d. Visual grounding: Phrase



Mark the area where you observe: *marked elongation and increased caliber of the thoracic aorta*.



The area specified is at coordinates [0.39, 0.3, 0.66, 0.79].



Figure 1: Examples of single instructions for different tasks. We design three main types of instructions based on dataset attributes. For datasets containing image-reports pairs (e.g., MIMIC-CXR), we design Q&A towards report generation (a). The instructions for datasets containing abnormality labels (e.g., CheXpert) are designed to perform multi-class classification (b). When bounding boxes are available, we design visual grounding instructions, where the assistant provides the bounding box coordinates to display them on the input image (c,d).

For this task, the instructions are designed such that the user asks the assistant to generate a report for a given CXR, and the assistant responds with the filtered report corresponding to that CXR (Figure 1a).

3.1.2 Abnormality classification

Another essential task an AI-assistant should be capable of is to identify the presence of abnormalities on a CXR. While simpler than generating detailed, unstructured observations, this functionality serves as a quick and helpful overview for physicians, highlighting key observations before they dive into a more detailed analysis.

For this task, we collect CXR datasets paired with abnormality labels. These labels were extracted from the original textual reports via the CheXbert automatic labeling tool (Smit et al., 2020), which identifies whether each of 14 possible abnormalities is present, absent, or uncertain. In our setup, we only consider frontal images and—in line with previous work (Yang et al., 2024b; Chaves et al., 2024)—consider “uncertain” abnormalities as “absent”.

For this task, we use 191,027 image-labels pairs from CheXpert (Irvin et al., 2019) and 237,912 pairs from MIMIC-CXR (Table 1). The instructions are designed such that the user asks for the abnormalities present on the CXR and the assistant answers by providing the list of abnormalities (Figure 1b).

3.1.3 Visual grounding

Detecting the location of specific anatomical regions or pathologies on a CXR is an important task for AI assistants. In addition to providing a textual description of the image, they should be able to spot where specific observations are located. This is usually done by predicting bounding box coordinates of top-left and bottom-right corners $[x_1, y_1, x_2, y_2]$. While classical object detectors (Ren et al., 2016; Redmon, 2016) tackle this task by leveraging specialized architectures and learning rules, we embark on it with the other text-based tasks via next-token prediction (Equation 1), formatting coordinates into text, enclosed between square brackets. As input images are pre-processed to a unique size by the vision encoder, we normalize these coordinates to the original dimension to obtain floating values between 0 and 1, similarly as in You et al. (2023); Park et al. (2024); Zhang et al. (2024a).

Task	Dataset source	Image-instruction pairs (#)	Evaluation (#)
Report Generation	MIMIC-CXR	$232,344 \times 1$	3,282
	CheXpert-Plus	$178,368 \times 1$	-
Abnormality classif.	MIMIC-CXR	$237,912 \times 1$	518
	CheXpert	$191,027 \times 1$	-
Anatomical grounding	Chest Imagenome	$80,000 \times 1$	2,000
Abnormality grounding	VinDr-CXR	$16,089 \times 3$	2,108
Abnormality detection	VinDr-CXR	$15,000 \times 2$	-
Phrase grounding	MS-CXR	971×3	189
	PadChest-GR	4478×2	-
Conversation	MIMIC-CXR	$80,312 \times 1$	523
Conversation (grounded)	MS-CXR	858×4	157
	PadChest-GR	$2,225 \times 4$	-

Table 1: Overview of the instruction dataset. The instruction dataset comprises 1,022,742 image-instruction pairs spanning multiple vision-language tasks, including report generation, abnormality classification, anatomical and abnormality grounding, phrase grounding, and conversational interactions. Dataset sources and the corresponding number of image-instruction pairs are listed, with smaller datasets balanced by varying the frequency of instruction occurrences.

The following datasets, with fine-grained X-ray information, were collected to design visual grounding instructions:

Chest Imagenome (Wu et al., 2021), derived from MIMIC-CXR, provides additional annotations to frontal X-ray images, in particular, bounding box coordinates for 29 anatomical regions. In our training data, we randomly select one region per image for each datapoint and create an instruction for anatomical region grounding following Figure 1.

VinDr-CXR (Nguyen et al., 2022) contains 18,000 frontal images, each manually annotated by three different radiologists. To merge their annotations, we pre-processed them by fusing bounding boxes of the same pathology using weighted box fusion (Solovyev et al., 2021), similarly as in Müller et al. (2024). From this dataset, we design two types of tasks: i) abnormality grounding, asking for the location of a specific abnormality (also following Figure 1c) and ii) abnormality detection, asking the location of all abnormalities, if any (Table 1).

MS-CXR (Boecking et al., 2022) provides image-sentence pairs of bounding boxes and corresponding phrases, complementing MIMIC-CXR.

PadChest-GR (Castro et al., 2024) also contains grounded sentences derived from the PadChest dataset (Bustos et al., 2020).


From the last two datasets, we construct the ‘phrase grounding’ task, where a user asks about the location of a specific sentence from a radiology report, and the assistant provides its associated bounding box coordinates (Figure 1d).


3.1.4 Conversations

Fine-tuning a VLM on single instructions, as presented above, is useful to acquire maximal precision in specific tasks but would not be sufficient to build a robust, flexible, and conversational radiology assistant. First, in a real-life setting, we cannot assume that physicians prompt the model with a limited set of instructions. Various types of questions could be posed, such as asking about the characteristics of a specific organ (lungs, heart), the orientation of the X-ray, or the definition of certain medical terms. More importantly, interactions can be decomposed over several Q&A rounds, with sometimes a question referring to previous answers (e.g., asking about the location of a specific observation from the previous answer). The model should thus be tuned to sequentially connect visual concepts (textual observations, presence or absence of abnormalities, fine-grained information) throughout a single conversation thread.


To develop this capability in RadVLM, we constructed an instruction-tuning dataset mimicking a real-life multi-turn interaction between user and assistant, named “conversation dataset”. Here, questions can be asked in different order, and the assistant reacts to the content of previous answers. Inspired by the vision-language models LLaVA (Liu et al., 2023) and LLaVA-Med (Li et al., 2023a), we prompt a larger text-only LLM (GPT-

a. Sample conversation


 Can you describe what you see in the chest X-ray?




Sure, I see a chest X-ray taken from the front view, known as AP (anterior-posterior). The heart appears to be borderline enlarged, but otherwise, the mediastinal and hilar regions look normal. There are no signs of fluid around the lungs or collapsed lung areas.

 Is there anything unusual in the lung area?


The lungs mostly look clear, but there is some linear scarring or atelectasis in the right lung base. Apart from that, the lung fields do not show any significant abnormalities.

 Are there any signs of past surgery visible in the X-ray?

Yes, there are clips visible in the right upper quadrant of the abdomen, which are often left after a cholecystectomy, a surgical procedure to remove the gallbladder.


 Does the X-ray show any signs of fluid around the lungs?


No, the X-ray does not show any signs of pleural effusion, which is fluid accumulation around the lungs.

 Is the heart looking normal in size and shape?


The heart size appears borderline enlarged, which means it is slightly bigger than expected, but not significantly abnormal in shape.

b. Sample conversation with grounding


 Can you tell me what you observe in this chest X-ray?




The X-ray shows that the cardiac silhouette is enlarged. There is also suspicion of mild left basal atelectasis.


 Where is the cardiac silhouette enlargement located on the image?

The enlarged cardiac silhouette is located within the coordinates [0.51, 0.43, 0.98, 0.79].




 Is there any fluid accumulation in the pleural space visible in the X-ray?

No, there is no visible pleural effusion on the X-ray.

 What can be said about the right lung in this image?

The right lung appears clear with no visible abnormalities.

 What does atelectasis mean?

Atelectasis refers to the partial collapse or incomplete inflation of the lung. In this X-ray, mild left basal atelectasis is suspected at the base of the left lung.

Figure 2: Example of LLM-generated conversations within the instruction dataset. LLM-generated user-assistant interactions designed for instruction tuning in RadVLM, covering both standard conversations and grounded responses. **(a) Standard conversation:** The assistant responds to user queries based on textual attributes extracted from the CXR (e.g., report findings, categorical labels) without explicit spatial references. **(b) Conversation with grounding:** In addition to textual responses, the assistant provides spatial grounding by referencing anatomical structures with bounding box coordinates. These synthetic interactions are generated by conditioning a text-based LLM on CXR attributes (report, labels, bounding boxes) and prompting it to simulate multi-turn diagnostic dialogues.

4o-mini) to generate multi-turn conversations. The prompt includes a system message instructing the LLM to generate a dialogue between a user and an assistant, along with detailed CXR information – including the radiology report, abnormality labels, bounding box coordinates, view, and gender (see prompt in [Appendix-Figure 1](#)). Importantly, by leveraging the provided CXR information, the assistant is designed to respond as if it had direct visual access to the image ([Figure 2](#)).

Following this process, we generate in total 83k image-conversation pairs, including 80k standard conversations ([Figure 2a](#)) and 3k “grounded conversations” ([Figure 2b](#)) that include interactions aimed at localizing specific observations. For the grounded conversations, it is essential to supply pairs of textual observations and their corresponding bounding box coordinates in the prompt. To achieve this, we use the datasets used for the “phrase grounding” task, MS-CXR and PadChest-GR, that provide annotations linking specific phrases in radiology reports to precise image location. We thereby obtain 858 image-conversation pairs derived from MS-CXR grounded phrases, and 2,225 pairs derived from PadChest-GR ([Table 1](#)).

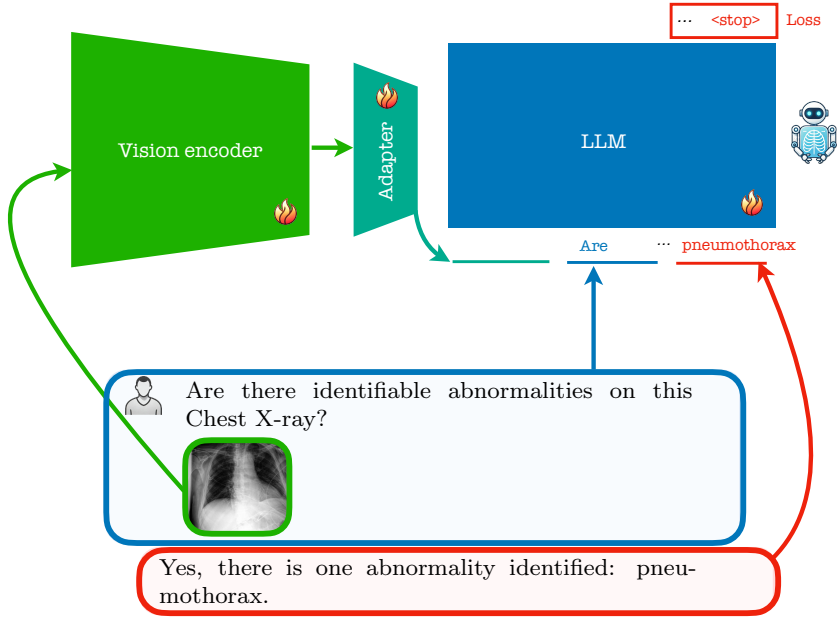


Figure 3: Instruction fine-tuning of the vision-language model. The CXR image is processed by the vision encoder, and the question is supplied at the language decoder. The flame icons indicate that the vision encoder, adapter, and LLM are all jointly fine-tuned end-to-end, generating the answer through next-token prediction.

3.2 Model finetuning

We leverage an existing vision-language backbone, LLaVA-OneVision-7B (Li et al., 2024). Its architecture is based on the SigLIP vision encoder (Zhai et al., 2023) connected to the language model qwen-2 (Yang et al., 2024a) via a 2-layer multi-layer perceptron (MLP). It was originally pretrained and instruction-tuned on image-text datasets in the general domain. We also follow the Higher AnyRes strategy (Chai et al., 2022) by encoding multiple patches of the input image in different resolutions (in addition to the full image) and feeding the concatenated output representation from the vision encoder to the language model. Chai et al. (2022) showed that the scaling in image resolution is successful in the general domain.

We fine-tune the LLaVA-OneVision-7B architecture on our instruction dataset by optimizing an auto-regressive loss on the target assistant tokens, \mathbf{x}_a . Specifically, for each token x_i in the assistant’s output sequence, we model

$$p(\mathbf{x}_a | \mathbf{x}_v, \mathbf{x}_q) = \prod_{i=1}^L p(x_i | \mathbf{x}_v, \mathbf{x}_{q,<i}, \mathbf{x}_{a,<i}), \quad (1)$$

where \mathbf{x}_v denotes the visual tokens, and $\mathbf{x}_{q,<i}$ and $\mathbf{x}_{a,<i}$ represent the question and assistant tokens preceding token x_i , respectively. Here, L is the number of tokens in the target assistant sequence. This formulation also applies for the multi-turn conversations, where $\mathbf{x}_{q,<i}$ and $\mathbf{x}_{a,<i}$ include the chat history from previous rounds. Following recent trends in visual instruction tuning (Li et al., 2024; Laurençon et al., 2024), the whole architecture is trained, using a learning rate of $2e-6$ in the vision encoder weights and $1e-5$ in the 2-layer MLP and language model weights. RadVLM is trained over 1 epoch of the instruction dataset using full-fine-tuning. We use 128 GH GPUs, each with 96GB of memory (Fusco et al., 2024) for approximately 12 hours.

For the ablation studies, we follow the same fine-tuning procedure but limit the process to a subset of the instruction dataset, focusing on isolated types of tasks.

4 Experiments & Results

In this section, we describe our evaluation pipeline, the existing baseline models we use for comparison, report results and highlight the capabilities of our RadVLM system.

4.1 Evaluation pipeline

In order to assess the quantitative performance of RadVLM, we design an evaluation pipeline based on the individual tasks from our instruction dataset. This pipeline leverages existing metrics for report generation, abnormality classification and visual grounding and creates novel evaluation tasks to assess the model’s performance in conversational abilities.

4.1.1 Report generation

To evaluate generated reports, we employ both lexical and radiology-specific metrics. Lexical metrics particularly quantify word overlap between generated and ground truth reports, among which we report BertScore, a metric for text generation based on computing token similarity using contextual embeddings (Zhang et al., 2020), and Rouge-L (Lin, 2004), which quantifies the length of the longest common subsequence between predicted and reference reports.

In contrast with lexical metrics, radiology-specific metrics ignore irrelevant variations in phrasing and focus on the clinically relevant semantics of the generated text, such as the presence or absence of an abnormality. In particular, we provide results for the RadGraph F1 and GREEN metrics.

RadGraph F1 (Delbrouck et al., 2022; Yu et al., 2023a): computing this metric requires to map each generated and ground truth reports to a structured graph, named RadGraph (Jain et al., 2021), containing radiology-specific entities (anatomy or observations) and the relations between them (“suggestive of”, “located at”). The RadGraph F1 score (Delbrouck et al., 2022) computes the overlap in inferred structured graphs (extracted entities and relations) from both generated and ground truth reports. In our study, we use the recently released RadGraph-XL model to extract graphical representations (Delbrouck et al., 2024) and report the partial reward (described in Delbrouck et al., 2022).

GREEN (Generative Radiology Report Evaluation and Error Notation, Ostmeier et al., 2024): a recently developed report generation metric that leverages the LLM-as-Judge mechanism of language models (Zheng et al., 2023b) to identify clinically significant errors in generated radiology reports (Yu et al., 2023b; Calamida et al., 2023, 2024), and that highly aligns with expert preferences as compared to other LLM-based evaluations (e.g., GPT-4).

4.1.2 Abnormality classification

We use the test split of the CheXpert dataset and prompt the model by asking to list the abnormalities present on the CXR. The mentioned abnormalities in the model’s answer are extracted via key-word matching and compared to the ground truth list. We calculate the F1 score for the 14 abnormalities and report the macro-averaged F1-score over all categories.

4.1.3 Visual grounding

We assess the model’s performance in visual grounding by prompting the model to detect specific features (anatomy, abnormality, phrase) and extract the bounding box coordinates generated within the model’s answer. Although we included the abnormality detection task in the instruction set, we do not evaluate it here due to the lack of comparable models for this task.

For the three grounding tasks, we use mean Average Precision (mAP) at an Intersection Over Union (IoU) threshold of 0.5. At this setting, we evaluate both precision and recall for predicted boxes that overlap with ground truth by at least 50%.

4.1.4 Multi-turn evaluation within conversational interactions

Evaluating conversational aspects of a model is essential to assess the utility and performance of an AI assistant in a multi-turn setting. We designed an LLM-based evaluation method carefully crafted for conversations, following the “LLM-as-judge” scheme (Zheng et al., 2023b) previously adopted by LLaVA-Med (Li et al., 2023a). We created a test set of conversations following our generation process (see Section 3.1.4). For this test set, we used GPT-4o instead of GPT-4o-mini (which was used for the training set) to ensure a higher quality of generated conversations, ensuring that the computed performance metrics accurately reflect the VLM’s capabilities rather than limitations in the test set. As a result, we obtained 157 conversations containing grounding questions (derived from MS-CXR test set), and 523 conversations without (Table 1).

During the evaluation process, we provide the CXR image to the VLM and sequentially ask the questions from this dataset. After collecting the VLM’s answer to each question, we prompt GPT-4o (text-only) with the CXR information (report, list of abnormalities, etc.), the expected answer per question (derived from the ground truth information), and the VLM-generated answer (see [Appendix-Figure 2](#) for the prompt). At the end of the prompt, GPT-4o is asked to provide an overall score (from 0 to 10) for the quality and accuracy of generated answers as compared to ground truth. We report two scores: one based on the grounded conversations dataset and one based on the non-grounded (standard) one.

4.2 Baseline models

Model	Size	Report	Classification	Grounding	Conversation
LLaVA-OV	7B	✓	✗	✗	✓
LLaVA-Med	7B	✓	✗	✗	✓
RaDialog	7B	✓	✓	✗	✓
CheXagent	3B	✓	✓	✓	✗
MAIRA-2	13B	✓	✗	✓	✗
RadVLM	7B	✓	✓	✓	✓

Table 2: Functional capabilities of RadVLM and baseline models. Comparison of RadVLM with baseline models in terms of parameter size and task coverage across report generation, abnormality classification, visual grounding and conversational interactions.

To provide insights into the performance of RadVLM in multiple tasks, we compare the instruction-tuned RadVLM to existing and publicly available state-of-the-art VLMs (from 3B to 13B, [Table 2](#)), adjusting the evaluation so that each baseline model is only tested on tasks for which it was initially trained on. Notably, in the general domain, we evaluate LLaVA-OneVision-7B ([Li et al., 2024](#)), also used as our training starting point (Section [3.2](#)). In the medical domain, we evaluate LLaVA-Med ([Li et al., 2023a](#)), trained on a large-scale biomedical dataset (including CXRs). For CXR-specific VLMs, we use CheXagent (trained on a wide range of tasks), RaDialog (possessing conversation skills), and MAIRA-2 ([Bannur et al., 2024](#)), specialized in report generation with visual grounding. We summarize the tasks on which each model is evaluated on in [Table 2](#), and provide links to the original repositories from which the model weights were obtained in [Appendix-Table 1](#).

4.3 Results

4.3.1 Report generation

Firstly, we evaluate RadVLM on a core radiology task: generating a textual report from a frontal CXR. As our evaluation set, we use a filtered version of the MIMIC-CXR test set, excluding statements about findings from prior examinations. We report in [Table 3](#) both lexical (BertScore, Rouge-L) and clinical (RadGraph F1, GREEN) metrics, which capture different performance aspects of the report generation task.

As mentioned in Section [4.2](#), five additional VLMs – including three specific to CXR (RaDialog, CheXagent, MAIRA-2) – are also evaluated, with minor adaptations to each model’s recommended prompt template. Many of these models were originally evaluated under different conditions (sometimes benefiting from extra inputs like prior images/reports or patient details or omitting certain metrics such as GREEN). To ensure that our setup remains consistent across all of them, we apply the same evaluation pipeline (test set and metrics).

For non-CXR specific VLMs, we observe a poor performance in both lexical and clinical metrics, with an unexpected improved performance for the generalist model (LLaVA-OneVision) over the medical one (LLaVA-Med), presumably profiting from a better architecture and training process ([Li et al., 2024](#)). CXR-specific models perform significantly better than generalists, with a notable advantage of CheXagent in terms of clinical metrics. While MAIRA-2 was shown to perform optimally in the report generation task ([Bannur et al., 2024](#)), it seems to perform worse when a single image is provided. Overall, RadVLM achieves competitive results, attaining the highest performance in lexical metrics and the second-best in clinical metrics. This validates our approach, even though our training methodology was not specifically designed for the report generation task.

4.3.2 Abnormality classification

In this section, we assess each model’s ability to predict which abnormalities are visible on the CXR. We use the manually curated CheXpert test set, prompt RadVLM to list any observed abnormalities, and compare them against the ground truth. As for the report generation task, we adapt the prompt for each compared

	NLG Metrics (%)		Clinical Metrics (%)	
	BertScore	Rouge-L	RadGraph F1	GREEN
LLaVA-OV	35.5	14.6	7.2	11.9
LLaVA-Med	30.1	12.6	4.7	5.0
RaDialog	49.7	22.4	16.3	24.4
CheXagent	38.1	<u>22.9</u>	20.9	28.5
MAIRA-2	<u>47.9</u>	18.5	13.5	21.4
RadVLM	51.0	24.3	<u>17.7</u>	<u>24.9</u>

Table 3: Performance of RadVLM and baseline models on single-image report generation. NLG (Natural Language Generation) and clinical metrics are calculated on the filtered test set of MIMIC-CXR. Bold values indicate the best performance, while underlined values represent the second-best performance across models.

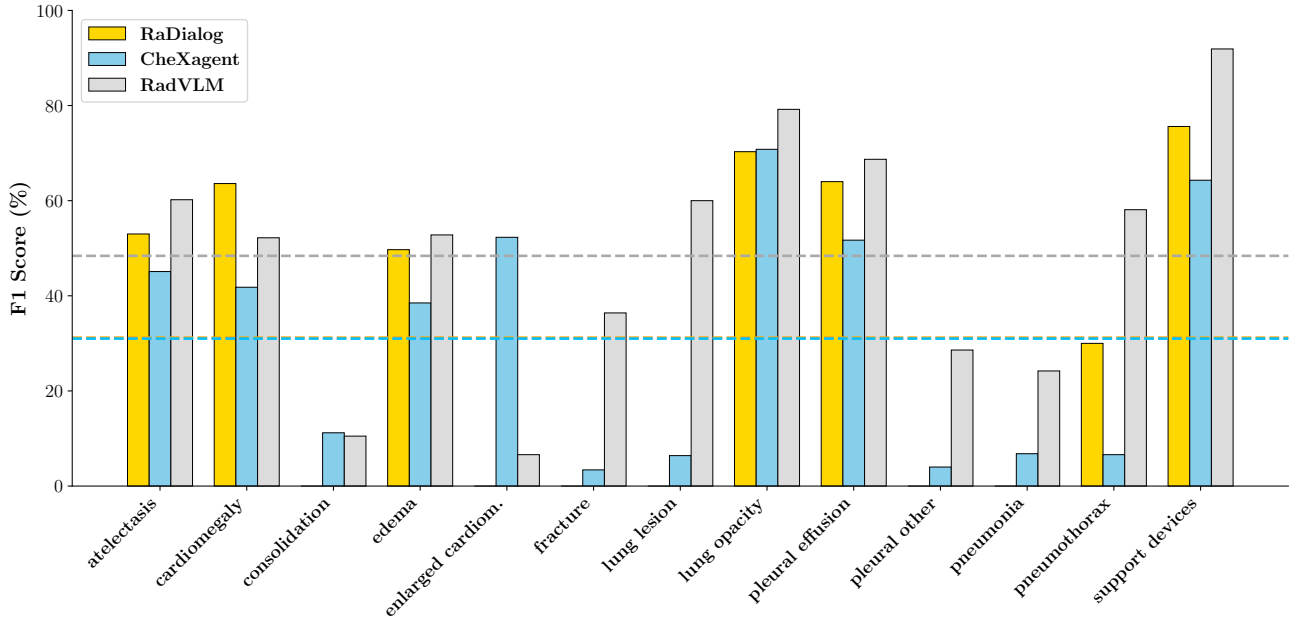


Figure 4: F1 scores for abnormality classification across different models. Classification performance of RadVLM (grey), RaDialog (yellow), and CheXagent (blue). Bars represent the F1 scores for individual pathology categories, while dashed lines indicate the macro-averaged F1 score across all categories. The macro-averaged F1 scores for CheXagent and RaDialog overlap.

baseline model (RaDialog, CheXagent) so they output a full list of abnormalities. Notably, RaDialog can identify pathologies from the same prompt as RadVLM, whereas CheXagent needs all possible labels explicitly listed in its prompt.

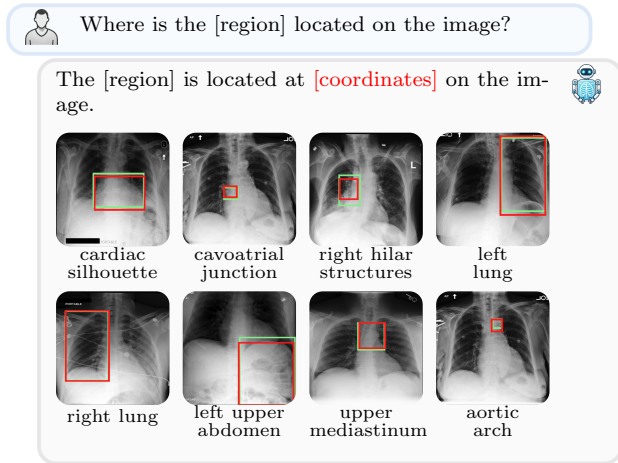
Figure 4 shows the individual F1 scores for the 14 CheXpert labels as well as the macro-averaged F1 across all categories (dashed lines in Figure 4). Our findings suggest that RadVLM better captures which abnormalities appear on the CXR, reflected in its higher macro-F1 score. In particular, it shows improved classification for crucial pathologies such as atelectasis, edema, fracture, lung lesion, lung opacity, pneumonia, pleural effusion, and pneumothorax. While CheXagent showed strong classification results under binary or restricted-label evaluations (Chen et al., 2024), it struggles when tasked with identifying all categories at once (see Figure 4).

Overall, these results indicate that RadVLM performs equally or better than its counterparts in abnormality classification. This step is especially crucial for the grounding process since identifying the relevant pathology is a prerequisite to localizing it on the CXR.

4.3.3 Visual grounding

In this section, we evaluate RadVLM’s visual grounding capabilities, which could help clinicians localize specific regions or pathologies on a CXR. This is particularly useful once a pathology has already been identified – either by a radiologist’s input or through our previously described AI tasks – since it allows one to pinpoint exactly where the abnormality appears on the image.

a. Anatomical grounding



b. Abnormality grounding

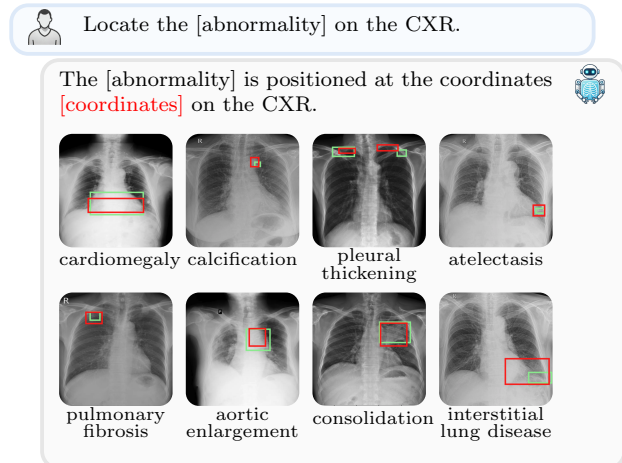


Figure 5: CXR region and abnormality grounding with RadVLM. Examples of RadVLM’s grounding predictions for (a) anatomical regions and (b) abnormalities in CXR images. The model predicts bounding boxes indicating the location of queried structures or pathological findings. Green boxes represent ground truth annotations, while red boxes denote model-predicted bounding boxes.

	Anatomical grounding	Abnormality grounding	Phrase grounding
CheXagent	6.2	<u>26.0</u>	69.7
MAIRA-2	<u>19.8</u>	11.3	<u>80.1</u>
RadVLM	85.3	35.7	82.8

Table 4: Visual grounding performance measured in mAP (%). Mean average precision (mAP) scores for anatomical grounding, abnormality grounding, and phrase grounding tasks across different models. Bounding box coordinates are extracted from each model’s output, and mAP is computed using an IoU threshold of 50%. **Bold** values indicate the highest performance, while underlined values represent the second-best performance.

We report performance metrics for the three main grounding tasks RadVLM was trained on: anatomical grounding using the Chest Imagenome test set, abnormality grounding using the VinDr-CXR test set, and phrase grounding using the MS-CXR test set (Table 1). For each task, we use mean Average Precision (mAP) as our primary evaluation metric.

As mentioned in Table 2, some of the CXR-specific VLMs already have grounding capabilities. CheXagent was trained to handle both abnormality and phrase grounding tasks, while MAIRA-2 – originally trained to produce radiology reports with grounded observations – is also capable of predicting bounding box coordinates when provided with input text (see corresponding model card in Appendix-Table 1). After retrieving each model’s instruction template for generating bounding box coordinates, we evaluated both CheXagent and MAIRA-2 on all three grounding tasks performed by RadVLM.

Our results show that RadVLM performs well at localizing anatomical regions (e.g., “right lung”, “aortic arch”, illustrated in Figure 5a), achieving a mAP of 85.3 %, by far surpassing the other CXR grounding models (Table 4). This advantage is partly explained by including the Chest Imagenome dataset (and thus the anatomical grounding task) in the training set, which CheXagent and MAIRA-2 did not leverage. However, it remains a key feature for any grounding model to possess a fine-grained understanding of CXR anatomy.

For the abnormality grounding task, RadVLM is less consistent (Figure 5b), likely due to higher sparsity of abnormality locations and labels, yet it still achieves best performance (Table 4). For the phrase grounding task, while MAIRA-2 and CheXagent demonstrate great performance, RadVLM surpasses them with a mAP of 82.8% (Table 4), presumably benefiting from the newly released PadChest-GR dataset (Castro et al., 2024) used for training.

Overall, these results show that our instruction tuning strategy for visual grounding (covering three essential tasks), combined to a modern VLM backbone, offers a promising avenue to help clinicians localize anatomical and pathological features during a CXR exam. Furthermore, providing fine-grained details within an LLM-generated output may also enhance the ability to answer grounded questions in a multi-turn setting, as we explore next.

Model	GPT-4o Score	GPT-4o Score w/ grounding
LLaVA-OV	4.66	3.85
LLaVA-Med	4.01	3.43
RaDialog	<u>4.57</u>	<u>4.09</u>
RadVLM	6.95	6.55

Table 5: Conversation performance on standard and grounded interactions. GPT-4o evaluation scores for conversational performance across models, comparing generated responses to expected answers derived from image-based attributes (e.g., reports, bounding boxes, and view type). Scores are reported for standard conversations and grounded conversations, where models must provide spatially aware responses. **Bold** values indicate the best performance, while underlined values represent the second-best performance.

4.3.4 Conversational abilities

Our model can already handle multiple advanced tasks for CXR interpretation. However, we have only tested its ability to follow instructions in a single-turn, question-answer format so far. An essential aspect of a VLM’s performance is also its capacity to manage follow-up questions in a multi-turn exchange with the user. Simply generating a full report or marking image features in one shot does not necessarily imply that the model can handle a varied sequence of precise questions – covering observations, locations, clarifications of medical terms, and more.

RadVLM’s instruction dataset also includes image-conversation pairs (Figure 2) generated with GPT-4o-mini, by providing it with a radiology report, any available grounded phrases, and additional details. As mentioned in Section 4.1.4, we created two held-out evaluation sets using GPT-4o: one without grounded questions and one focused on grounded questions derived from the MS-CXR test set (Table 1). We run the evaluation on both test sets and report the average score across all samples. We also evaluate the other baseline models that possess conversational abilities, thoroughly respecting their prompting template within a multi-turn setting. The average GPT-4o scores for RadVLM and other models are gathered in Table 5.

Our results show that RadVLM, trained on a broad range of image-conversation pairs, achieves an average score of 6.95/10, substantially higher than the other conversational models, whose responses often prove incorrect or vague (Figure 6). This advantage may stem from RadVLM’s ability to handle varied question types and sequences in multi-turn exchanges, a skill reinforced by the sparse nature of its training conversations. The gap becomes even more pronounced in grounded scenarios, where RadVLM maintains strong performance (6.55/10) while others drop even more. Notably, this suggests that even the limited number of grounded conversations included (Table 1) was sufficient to equip RadVLM with robust grounding capabilities in a multi-turn setting.

4.4 Ablation studies

In this section, we investigate a fundamental question in LLM fine-tuning: do models perform individual tasks more effectively when they are trained separately, or does joint training on multiple tasks provide a greater overall benefit? To address this question, we perform ablation studies where we train separate models – each dedicated to a single task (e.g., report generation, classification) – using the same training settings and hyperparameters as RadVLM, then evaluate their performance on that respective task.

Our results reveal that RadVLM generally outperforms models trained on individual tasks. First, this difference is pronounced in grounding performance, particularly for tasks with smaller training sets (e.g., phrase grounding; see Table 1). We attribute this to the complementary nature of the various grounding tasks, which collectively improve the model’s ability to localize visual elements (including overlapping categories, such as “abnormalities” also mentioned in “phrases”) and prevent overfitting.

A similar trend emerges in the conversation scores, where RadVLM outperforms a model trained solely on the conversation dataset. While this ablated model still performs significantly better than its baseline backbone – surpassing LLaVA-OneVision’s score in Table 2 – RadVLM leverages knowledge from the other tasks, such as report generation, that contains a higher amount of data points. This presumably enables it to generalize more effectively to new questions from the conversation test set.

Report generation is the only task that turns out equivalent when trained in isolation. One likely reason is the high amount of training data for this task, and the richness of information textual reports contain over other tasks, which might suffice for the model to generalize over new instances.

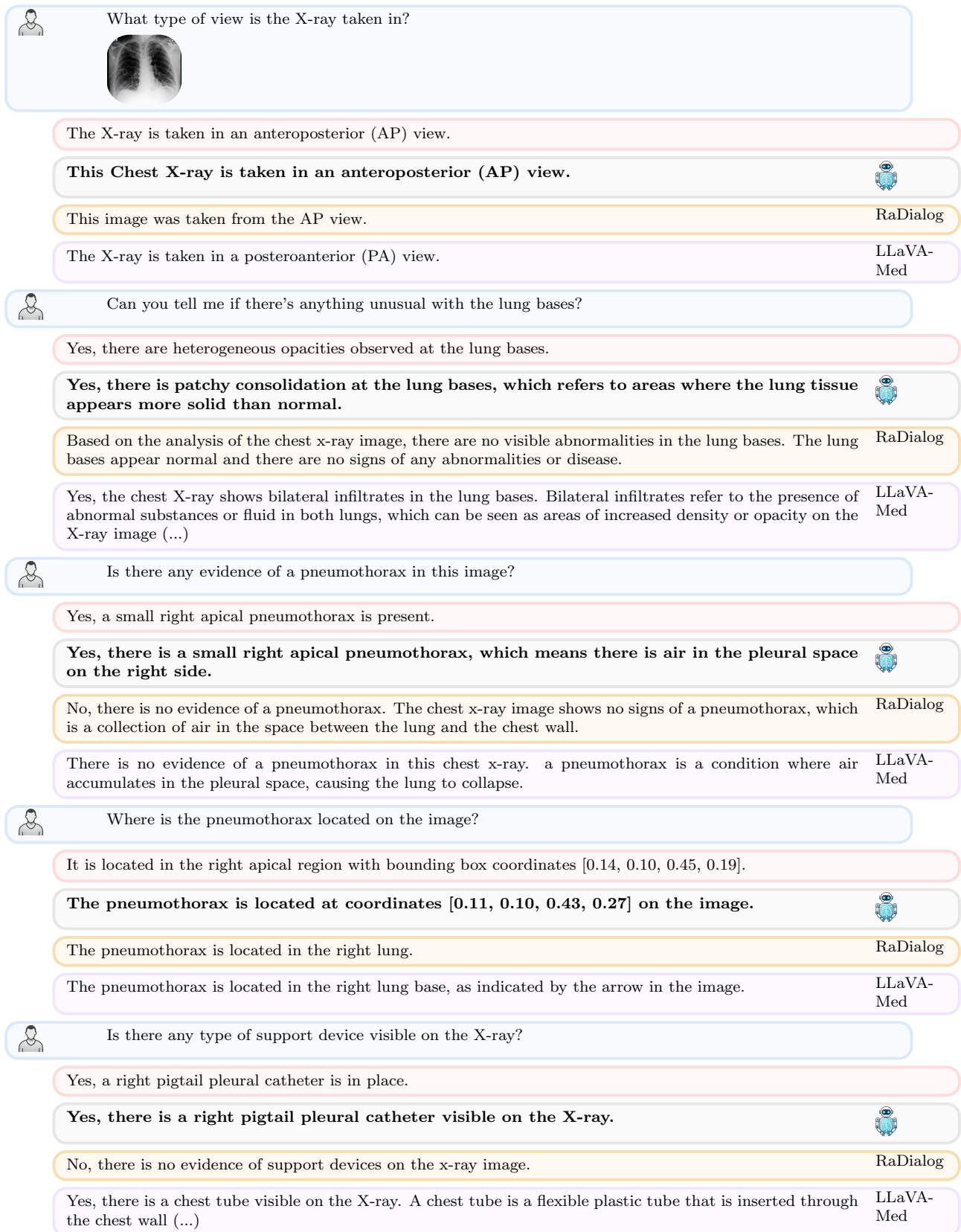


Figure 6: Example of multi-turn interaction with RadVLM and other conversational VLMs. Comparison of expected answers from the **conversation dataset** (red bubbles) to generated answers from RadVLM (grey bubble), **RaDialog** (yellow bubble), and **LLaVA-Med** (purple bubble).

Training tasks	Evaluation tasks					
	Report generation	Classification	Anatomical grounding	Abnormality grounding	Phrase grounding	Conversation (standard/grounded)
	RadGraph/GREEN	F1 (macro) (%)	mAP (%)	mAP (%)	mAP (%)	GPT4o-Score
Report generation	17.7 / 25.4	-	-	-	-	-
Classification	-	41.5	-	-	-	-
Anatomical grounding	-	-	83.0	-	-	-
Abnormality grounding	-	-	-	27.1	-	-
Phrase grounding	-	-	-	-	64.6	-
Conversation	-	-	-	-	-	6.28 / 5.66
All (RadVLM)	17.7 / 24.9	48.4	85.3	35.7	82.8	6.95 / 6.55

Table 6: Ablation studies comparing single-task models to RadVLM. Each ablated model is trained on only one task from RadVLM’s instruction dataset and evaluated on that same task. We compare these results to RadVLM’s previously reported performance over all tasks.

5 Conclusions

There is a growing need for medical AI tools that are both accurate and user-friendly, and can interact with clinicians in a natural, multi-turn conversation. In this study, inspired by advances in both general and CXR-specific vision-language models, we explored the potential of constructing an assistant that not only aims for strong performance in individual tasks but also for handling them in a multi-turn, interactive setting. To achieve this, we built an instruction dataset that integrates both stand-alone tasks and multi-task dialogues, then fine-tuned a VLM backbone on it. Our findings suggest that this method performs well and offers promising insights for designing future radiology assistants.

One key contribution of this study is our consistent re-implementation and evaluation of existing models (alongside RadVLM) under a unified experimental framework. In an era where AI research is proliferating rapidly, and new models are introduced almost daily, it can be challenging to compare results that rely on different setups. By systematically re-implementing models and replicating experiments within the same context, we enhance both reproducibility and reliability. This standardized approach aligns with initiatives such as the ReXrank leaderboard for CXR report generation (Zhang et al., 2024b), which similarly evaluates state-of-the-art models using a consistent protocol. Ultimately, these efforts provide a clearer understanding of each model’s true capabilities and help researchers identify the most promising directions for future work.

Another key takeaway is the flexibility of VLMs in handling diverse data types, ranging from free-text reports and classification labels to fine-grained information, all within a multi-turn, “real-life” scenario. Traditionally, each task might have been tackled by distinct, specialized architectures – e.g., separate object detectors (Sun and Cong, 2022) or classifiers (He et al., 2016) – but our findings support the recent trend, employed in both general and CXR-specific visual modeling (Lin et al., 2024; Wang et al., 2024; Sharma et al., 2024; Chen et al., 2024), where many data formats can now be tokenized and processed through a common next-token generation paradigm. Our ablation studies further show that while each task differs in purpose, they collectively enhance the model’s overall understanding of a CXR image, an effect likely amplified by training them together. Even though multi-agent approaches emerge in the medical setting (Schmidgall et al., 2024), these results support the value of joint training for developing comprehensive, single-agent solutions.

The simplicity of RadVLM’s training strategy also sheds light on potential directions for future CXR-based modeling. Here, we built upon LLaVA-OneVision (Li et al., 2024), a VLM already pretrained for instruction following, and fine-tuned it on our curated dataset for just a single epoch. Although other studies have employed more intricate pipelines, such as pre-training the vision encoder, adapter and LLM components successively (Chaves et al., 2024; Chen et al., 2024; Bannur et al., 2024), Given the competitive performance of RadVLM with other models, we hypothesize that the quality of the instruction dataset, coupled with the backbone architecture (as shown by Laurençon et al., 2024) are the most critical for the overall performance of such a visual foundation model. That said, for specific tasks like report generation, specialized solutions that incorporate additional patient details, prior and lateral images, or extended training, could offer greater gains. This likely explains why our model does not surpass the state of the art for that particular task. From this, we envision a future where AI assistants are bifurcated into (i) non-interactive, report-focused tools designed for experienced radiologists, and (ii) more adaptable, conversational agents that clinicians or radiology students can easily query in a multi-turn context.

As radiology datasets grow in both scale and quality, and as vision-language modeling advances at a rapid

pace, AI-driven tools are becoming ever more reliable and valuable for clinical practice. With RadVLM, we aim to contribute to this vibrant field by introducing a method that draws on prior work yet incorporates original ideas toward developing a multitask conversational vision-language model for radiology.

6 Acknowledgments

This work was supported as part of the Swiss AI Initiative by a grant from the Swiss National Supercomputing Centre (CSCS) under project ID a02 on Alps, and by the LOOP Zurich as part of the application driver project supporting the LOOP Zurich Biomedical Informatics Platform (BMIP). ND and FN received research support from the Digitalization Initiative of the Zurich Higher Education Institutions (DIZH)- Rapid Action Call - under TRUST-RAD project. CB received research support from the Promedica Foundation, Chur, CH. TS is supported by the grant #2021-911 of the Strategic Focal Area “Personalized Health and Related Technologies (PHRT)” of the ETH Domain (Swiss Federal Institutes of Technology). HM, MN and KF are supported by JSPS KAKENHI (Grant Number: 23KK0148). AR is supported by the StimuLoop grant #1-007811-002 and the Vontobel Foundation. MV and SL are supported by the Swiss State Secretariat for Education, Research, and Innovation (SERI) under contract number MB22.00047. MK is supported by the UZH Global Strategy and Partnerships Funding Scheme and a Research Partnership Grant with China, Japan, South Korea and the ASEAN region (RPG 072023.18).

References

- Achiam, J., Adler, S., Agarwal, S., Ahmad, L., Akkaya, I., Aleman, F. L., Almeida, D., Altenschmidt, J., Altman, S., Anadkat, S., et al. (2023). Gpt-4 technical report. *arXiv preprint arXiv:2303.08774*.
- Akhter, Y., Singh, R., and Vatsa, M. (2023). Ai-based radiodiagnosis using chest x-rays: A review. *Frontiers in Big Data*, 6:1120989.
- Alfarghaly, O., Khaled, R., Elkorany, A., Helal, M., and Fahmy, A. (2021). Automated radiology report generation using conditioned transformers. *Informatics in Medicine Unlocked*, 24:100557.
- Anthropic (2024). Introducing the next generation of Claude. Anthropic News, <https://www.anthropic.com/news/claude-3-family>. Accessed: 2024-11-26.
- Bannur, S., Bouzid, K., Castro, D. C., Schwaighofer, A., Thieme, A., Bond-Taylor, S., Ilse, M., Pérez-García, F., Salvatelli, V., Sharma, H., Meissen, F., Ranjit, M., Srivastav, S., Gong, J., Codella, N. C. F., Falck, F., Oktay, O., Lungren, M. P., Wetscherek, M. T., Alvarez-Valle, J., and Hyland, S. L. (2024). MAIRA-2: Grounded radiology report generation. *arXiv [cs.CL]*.
- Bluethgen, C., Chambon, P., Delbrouck, J.-B., van der Sluijs, R., Połacin, M., Zambrano Chaves, J. M., Abraham, T. M., Purohit, S., Langlotz, C. P., and Chaudhari, A. S. (2024). A vision–language foundation model for the generation of realistic chest x-ray images. *Nature Biomedical Engineering*, pages 1–13.
- Boecking, B., Usuyama, N., Bannur, S., Castro, D. C., Schwaighofer, A., Hyland, S., Wetscherek, M., Naumann, T., Nori, A., Alvarez-Valle, J., et al. (2022). Making the most of text semantics to improve biomedical vision–language processing. In *European conference on computer vision*, pages 1–21. Springer.
- Brown, T. B. (2020). Language models are few-shot learners. *arXiv preprint arXiv:2005.14165*.
- Bustos, A., Pertusa, A., Salinas, J.-M., and De La Iglesia-Vaya, M. (2020). Padchest: A large chest x-ray image dataset with multi-label annotated reports. *Medical image analysis*, 66:101797.
- Calamida, A., Nooralahzadeh, F., Rohanian, M., Fujimoto, K., Nishio, M., and Krauthammer, M. (2023). Radiology-aware model-based evaluation metric for report generation. *arXiv preprint arXiv:2311.16764*.
- Calamida, A. R., Nooralahzadeh, F., Rohanian, M., Nishio, M., Fujimoto, K., and Krauthammer, M. (2024). Radiology report generation models evaluation dataset for chest x-rays (RadEvalX).
- Çallı, E., Sogancioglu, E., van Ginneken, B., van Leeuwen, K. G., and Murphy, K. (2021). Deep learning for chest x-ray analysis: A survey. *Medical Image Analysis*, 72:102125.
- Castro, D. C., Bustos, A., Bannur, S., Hyland, S. L., Bouzid, K., Wetscherek, M. T., Sánchez-Valverde, M. D., Jaques-Pérez, L., Pérez-Rodríguez, L., Takeda, K., et al. (2024). Padchest-gr: A bilingual chest x-ray dataset for grounded radiology report generation. *arXiv preprint arXiv:2411.05085*.

- Chai, L., Gharbi, M., Shechtman, E., Isola, P., and Zhang, R. (2022). Any-resolution training for high-resolution image synthesis. In *European Conference on Computer Vision*, pages 170–188. Springer.
- Chambon, P., Delbrouck, J.-B., Sounack, T., Huang, S.-C., Chen, Z., Varma, M., Truong, S. Q., Chuong, C. T., and Langlotz, C. P. (2024). Chexpert plus: Augmenting a large chest x-ray dataset with text radiology reports, patient demographics and additional image formats.
- Chaves, J. M. Z., Huang, S.-C., Xu, Y., Xu, H., Usuyama, N., Zhang, S., Wang, F., Xie, Y., Khademi, M., Yang, Z., Awadalla, H., Gong, J., Hu, H., Yang, J., Li, C., Gao, J., Gu, Y., Wong, C., Wei, M., Naumann, T., Chen, M., Lungren, M. P., Chaudhari, A., Yeung-Levy, S., Langlotz, C. P., Wang, S., and Poon, H. (2024). Towards a clinically accessible radiology foundation model: open-access and lightweight, with automated evaluation.
- Chen, Z., Varma, M., Xu, J., Paschali, M., Veen, D. V., Johnston, A., Youssef, A., Blankemeier, L., Bluethgen, C., Altmayer, S., Valanarasu, J. M. J., Muneer, M. S. E., Reis, E. P., Cohen, J. P., Olsen, C., Abraham, T. M., Tsai, E. B., Beaulieu, C. F., Jitsev, J., Gatidis, S., Delbrouck, J.-B., Chaudhari, A. S., and Langlotz, C. P. (2024). A vision-language foundation model to enhance efficiency of chest x-ray interpretation.
- Delbrouck, J.-B., Chambon, P., Bluethgen, C., Tsai, E., Almusa, O., and Langlotz, C. P. (2022). Improving the factual correctness of radiology report generation with semantic rewards. *arXiv preprint arXiv:2210.12186*.
- Delbrouck, J.-B., Chambon, P., Chen, Z., Varma, M., Johnston, A., Blankemeier, L., Van Veen, D., Bui, T., Truong, S., and Langlotz, C. (2024). Radgraph-xl: A large-scale expert-annotated dataset for entity and relation extraction from radiology reports. In *Findings of the Association for Computational Linguistics ACL 2024*, pages 12902–12915.
- Dubey, A., Jauhri, A., Pandey, A., Kadian, A., Al-Dahle, A., Letman, A., Mathur, A., Schelten, A., Yang, A., Fan, A., et al. (2024). The llama 3 herd of models. *arXiv preprint arXiv:2407.21783*.
- Feng, J., Sun, Q., Xu, C., Zhao, P., Yang, Y., Tao, C., Zhao, D., and Lin, Q. (2022). Mmdialog: A large-scale multi-turn dialogue dataset towards multi-modal open-domain conversation. *arXiv preprint arXiv:2211.05719*.
- Fusco, L., Khalilov, M., Chrapek, M., Chukkapalli, G., Schulthess, T., and Hoefler, T. (2024). Understanding data movement in tightly coupled heterogeneous systems: A case study with the grace hopper superchip. *arXiv preprint arXiv:2408.11556*.
- Guo, D., Yang, D., Zhang, H., Song, J., Zhang, R., Xu, R., Zhu, Q., Ma, S., Wang, P., Bi, X., et al. (2025). Deepseek-r1: Incentivizing reasoning capability in llms via reinforcement learning. *arXiv preprint arXiv:2501.12948*.
- He, K., Zhang, X., Ren, S., and Sun, J. (2016). Deep residual learning for image recognition. In *Proceedings of the IEEE conference on computer vision and pattern recognition*, pages 770–778.
- Homayounieh, F., Digumarthy, S., Ebrahimian, S., Rueckel, J., Hoppe, B. F., Sabel, B. O., Conjeti, S., Ridder, K., Sistermanns, M., Wang, L., Preuhs, A., Ghesu, F., Mansoor, A., Moghbel, M., Botwin, A., Singh, R., Cartmell, S., Patti, J., Huemmer, C., Fieselmann, A., Joerger, C., Mirshahzadeh, N., Muse, V., and Kalra, M. (2021). An artificial intelligence-based chest x-ray model on human nodule detection accuracy from a multicenter study. *JAMA Network Open*, 4:e2141096–e2141096.
- Hyland, S. L., Bannur, S., Bouzid, K., Castro, D. C., Ranjit, M., Schwaighofer, A., Pérez-García, F., Salvatelli, V., Srivastav, S., Thieme, A., et al. (2023). Maira-1: A specialised large multimodal model for radiology report generation. *arXiv preprint arXiv:2311.13668*.
- Irvin, J., Rajpurkar, P., Ko, M., Yu, Y., Ciurea-Ilcus, S., Chute, C., Marklund, H., Haghighi, B., Ball, R., Shpanskaya, K., et al. (2019). Chexpert: A large chest radiograph dataset with uncertainty labels and expert comparison. In *Proceedings of the AAAI conference on artificial intelligence*, volume 33, pages 590–597.
- Jain, S., Agrawal, A., Saporta, A., Truong, S. Q., Duong, D. N., Bui, T., Chambon, P., Zhang, Y., Lungren, M. P., Ng, A. Y., et al. (2021). Radgraph: Extracting clinical entities and relations from radiology reports. *arXiv preprint arXiv:2106.14463*.
- Johnson, A. E., Pollard, T. J., Greenbaum, N. R., Lungren, M. P., Deng, C.-y., Peng, Y., Lu, Z., Mark, R. G., Berkowitz, S. J., and Horng, S. (2019). Mimic-cxr-jpg, a large publicly available database of labeled chest radiographs. *arXiv preprint arXiv:1901.07042*.
- Kang, S., Kim, D., Kim, J., Lee, H. K., and Hwang, S. J. (2024). Wolf: Large language model framework for cxr understanding. *arXiv preprint arXiv:2403.15456*.

- Kim, S., Nooralahzadeh, F., Rohanian, M., Fujimoto, K., Nishio, M., Sakamoto, R., Rinaldi, F., and Krauthammer, M. (2023). Boosting radiology report generation by infusing comparison prior. In Demner-fushman, D., Ananiadou, S., and Cohen, K., editors, *The 22nd Workshop on Biomedical Natural Language Processing and BioNLP Shared Tasks*, pages 50–61, Toronto, Canada. Association for Computational Linguistics.
- Laurençon, H., Tronchon, L., Cord, M., and Sanh, V. (2024). What matters when building vision-language models? *arXiv preprint arXiv:2405.02246*.
- Laurençon, H., Marafioti, A., Sanh, V., and Tronchon, L. (2024). Building and better understanding vision-language models: insights and future directions.
- Li, B., Zhang, Y., Guo, D., Zhang, R., Li, F., Zhang, H., Zhang, K., Li, Y., Liu, Z., and Li, C. (2024). Llava-onevision: Easy visual task transfer. *arXiv preprint arXiv:2408.03326*.
- Li, C., Wong, C., Zhang, S., Usuyama, N., Liu, H., Yang, J., Naumann, T., Poon, H., and Gao, J. (2023a). Llava-med: Training a large language-and-vision assistant for biomedicine in one day. *arXiv preprint arXiv:2306.00890*.
- Li, J., Li, D., Savarese, S., and Hoi, S. (2023b). Blip-2: Bootstrapping language-image pre-training with frozen image encoders and large language models. In *International conference on machine learning*, pages 19730–19742. PMLR.
- Lin, C.-Y. (2004). Rouge: A package for automatic evaluation of summaries. In *Text summarization branches out*, pages 74–81.
- Lin, J., Yin, H., Ping, W., Molchanov, P., Shoeybi, M., and Han, S. (2024). Vila: On pre-training for visual language models. In *Proceedings of the IEEE/CVF Conference on Computer Vision and Pattern Recognition*, pages 26689–26699.
- Liu, A., Feng, B., Xue, B., Wang, B., Wu, B., Lu, C., Zhao, C., Deng, C., Zhang, C., Ruan, C., et al. (2024). Deepseek-v3 technical report. *arXiv preprint arXiv:2412.19437*.
- Liu, H., Li, C., Wu, Q., and Lee, Y. J. (2023). Visual instruction tuning. *arXiv preprint arXiv:2304.08485*.
- Müller, P., Kaissis, G., and Rueckert, D. (2024). Chex: Interactive localization and region description in chest x-rays. *arXiv preprint arXiv:2404.15770*.
- Nguyen, H. Q., Lam, K., Le, L. T., Pham, H. H., Tran, D. Q., Nguyen, D. B., Le, D. D., Pham, C. M., Tong, H. T., Dinh, D. H., et al. (2022). Vindr-cxr: An open dataset of chest x-rays with radiologists’ annotations. *Scientific Data*, 9(1):429.
- NIH (n.d.). Pubmed. <https://pubmed.ncbi.nlm.nih.gov/>, Accessed: 2024-12-22.
- Nishio, M., Noguchi, S., Matsuo, H., and Murakami, T. (2020). Automatic classification between covid-19 pneumonia, non-covid-19 pneumonia, and the healthy on chest x-ray image: combination of data augmentation methods. *Scientific Reports 2020 10:1*, 10:1–6.
- Nooralahzadeh, F., Perez Gonzalez, N., Frauenfelder, T., Fujimoto, K., and Krauthammer, M. (2021). Progressive transformer-based generation of radiology reports. In Moens, M.-F., Huang, X., Specia, L., and Yih, S. W.-t., editors, *Findings of the Association for Computational Linguistics: EMNLP 2021*, pages 2824–2832, Punta Cana, Dominican Republic. Association for Computational Linguistics.
- OpenAI (2024). ChatGPT can now See, Hear, and Speak. OpenAI Blog, <https://openai.com/index/chatgpt-can-now-see-hear-and-speak/>. Accessed: 2024-11-26.
- Ostmeier, S., Xu, J., Chen, Z., Varma, M., Blankemeier, L., Bluethgen, C., Michalson, A. E., Moseley, M., Langlotz, C., Chaudhari, A. S., et al. (2024). Green: Generative radiology report evaluation and error notation. *arXiv preprint arXiv:2405.03595*.
- Ouyang, L., Wu, J., Jiang, X., Almeida, D., Wainwright, C., Mishkin, P., Zhang, C., Agarwal, S., Slama, K., Ray, A., et al. (2022). Training language models to follow instructions with human feedback. *Advances in neural information processing systems*, 35:27730–27744.
- Park, J., Kim, S., Yoon, B., Hyun, J., and Choi, K. (2024). M4cxr: Exploring multi-task potentials of multi-modal large language models for chest x-ray interpretation. *arXiv preprint arXiv:2408.16213*.
- Pellegrini, C., Özsoy, E., Busam, B., Navab, N., and Keicher, M. (2023). Radialog: A large vision-language model for radiology report generation and conversational assistance. *arXiv preprint arXiv:2311.18681*.

- Peng, B., Li, C., He, P., Galley, M., and Gao, J. (2023). Instruction tuning with gpt-4. *arXiv preprint arXiv:2304.03277*.
- Peng, Y.-C., Lee, W.-J., Chang, Y.-C., Chan, W. P., and Chen, S.-J. (2022). Radiologist burnout: trends in medical imaging utilization under the national health insurance system with the universal code bundling strategy in an academic tertiary medical centre. *European journal of radiology*, 157:110596.
- Radford, A., Wu, J., Child, R., Luan, D., Amodei, D., Sutskever, I., et al. (2019). Language models are unsupervised multitask learners. *OpenAI blog*, 1(8):9.
- Redmon, J. (2016). You only look once: Unified, real-time object detection. In *Proceedings of the IEEE conference on computer vision and pattern recognition*.
- Ren, S., He, K., Girshick, R., and Sun, J. (2016). Faster r-cnn: Towards real-time object detection with region proposal networks. *IEEE transactions on pattern analysis and machine intelligence*, 39(6):1137–1149.
- Röntgen, W. C. (1895). *Ueber eine neue Art von Strahlen*. Phys.-med. Gesellschaft.
- Saab, K., Tu, T., Weng, W.-H., Tanno, R., Stutz, D., Wulczyn, E., Zhang, F., Strother, T., Park, C., Vedadi, E., et al. (2024). Capabilities of gemini models in medicine. *arXiv preprint arXiv:2404.18416*.
- Schmidgall, S., Ziaei, R., Harris, C., Reis, E., Jopling, J., and Moor, M. (2024). Agentclinic: a multimodal agent benchmark to evaluate ai in simulated clinical environments. *arXiv preprint arXiv:2405.07960*.
- Shammari, M. A., Hassan, A., AlShamlan, N., Alotaibi, S., Bamashmoos, M., Hakami, A., Althunyan, A., Basager, S., Motabgani, S., Aljubran, S., and Alsaif, H. S. (2021). Family medicine residents’ skill levels in emergency chest x-ray interpretation. *BMC Family Practice*, 22.
- Sharma, H., Salvatelli, V., Srivastav, S., Bouzid, K., Bannur, S., Castro, D. C., Ilse, M., Bond-Taylor, S., Ranjit, M. P., Falck, F., et al. (2024). Maira-seg: Enhancing radiology report generation with segmentation-aware multimodal large language models. *arXiv preprint arXiv:2411.11362*.
- Singhal, K., Azizi, S., Tu, T., Mahdavi, S. S., Wei, J., Chung, H. W., Scales, N., Tanwani, A., Cole-Lewis, H., Pfohl, S., et al. (2023). Large language models encode clinical knowledge. *Nature*, 620(7972):172–180.
- Smit, A., Jain, S., Rajpurkar, P., Pareek, A., Ng, A. Y., and Lungren, M. P. (2020). Chexbert: combining automatic labelers and expert annotations for accurate radiology report labeling using bert. *arXiv preprint arXiv:2004.09167*.
- Solovyev, R., Wang, W., and Gabruseva, T. (2021). Weighted boxes fusion: Ensembling boxes from different object detection models. *Image and Vision Computing*, 107:104117.
- Sun, K. X. and Cong, C. (2022). Research on chest abnormality detection based on improved yolov7 algorithm. In *2022 IEEE international conference on bioinformatics and biomedicine (BIBM)*, pages 3884–3886. IEEE.
- Tanida, T., Müller, P., Kaissis, G., and Rueckert, D. (2023). Interactive and explainable region-guided radiology report generation. In *Proceedings of the IEEE/CVF Conference on Computer Vision and Pattern Recognition*, pages 7433–7442.
- Team, G., Anil, R., Borgeaud, S., Alayrac, J.-B., Yu, J., Soricut, R., Schalkwyk, J., Dai, A. M., Hauth, A., Millican, K., et al. (2023). Gemini: a family of highly capable multimodal models. *arXiv preprint arXiv:2312.11805*.
- Tu, T., Palepu, A., Schaekermann, M., Saab, K., Freyberg, J., Tanno, R., Wang, A., Li, B., Amin, M., Tomasev, N., Azizi, S., Singhal, K., Cheng, Y., Hou, L., Webson, A., Kulkarni, K., Mahdavi, S. S., Semturs, C., Gottweis, J., Barral, J., Chou, K., Corrado, G. S., Matias, Y., Karthikesalingam, A., and Natarajan, V. (2024). Towards conversational diagnostic AI. *arXiv [cs.AI]*.
- Vaswani, A. (2017). Attention is all you need. *Advances in Neural Information Processing Systems*.
- Wang, P., Bai, S., Tan, S., Wang, S., Fan, Z., Bai, J., Chen, K., Liu, X., Wang, J., Ge, W., et al. (2024). Qwen2-vl: Enhancing vision-language model’s perception of the world at any resolution. *arXiv preprint arXiv:2409.12191*.
- Wang, Y., Kordi, Y., Mishra, S., Liu, A., Smith, N. A., Khashabi, D., and Hajishirzi, H. (2022). Self-instruct: Aligning language models with self-generated instructions. *arXiv preprint arXiv:2212.10560*.

- Wei, J., Bosma, M., Zhao, V. Y., Guu, K., Yu, A. W., Lester, B., Du, N., Dai, A. M., and Le, Q. V. (2021). Finetuned language models are zero-shot learners. *arXiv preprint arXiv:2109.01652*.
- Wu, J. T., Agu, N. N., Lourentzou, I., Sharma, A., Paguio, J. A., Yao, J. S., Dee, E. C., Mitchell, W., Kashyap, S., Giovannini, A., et al. (2021). Chest imagenome dataset for clinical reasoning. *arXiv preprint arXiv:2108.00316*.
- Yang, A., Yang, B., Hui, B., Zheng, B., Yu, B., Zhou, C., Li, C., Li, C., Liu, D., Huang, F., et al. (2024a). Qwen2 technical report. *arXiv preprint arXiv:2407.10671*.
- Yang, L., Xu, S., Sellergren, A., Kohlberger, T., Zhou, Y., Ktena, I., Kiraly, A., Ahmed, F., Hormozdiari, F., Jaroensri, T., et al. (2024b). Advancing multimodal medical capabilities of gemini. *arXiv preprint arXiv:2405.03162*.
- Yang, S., Wu, X., Ge, S., Zheng, Z., Zhou, S. K., and Xiao, L. (2023). Radiology report generation with a learned knowledge base and multi-modal alignment. *Medical Image Analysis*, 86:102798.
- You, H., Zhang, H., Gan, Z., Du, X., Zhang, B., Wang, Z., Cao, L., Chang, S.-F., and Yang, Y. (2023). Ferret: Refer and ground anything anywhere at any granularity. *arXiv preprint arXiv:2310.07704*.
- Yu, F., Endo, M., Krishnan, R., Pan, I., Tsai, A., Reis, E. P., Fonseca, E. K. U. N., Lee, H. M. H., Abad, Z. S. H., Ng, A. Y., et al. (2023a). Evaluating progress in automatic chest x-ray radiology report generation. *Patterns*, 4(9).
- Yu, F., Endo, M., Krishnan, R., Pan, I., Tsai, A., Reis, E. P., Kaiser Ururahy Nunes Fonseca, E., Lee, H., Shakeri, Z., Ng, A., Langlotz, C., Venugopal, V. K., and Rajpurkar, P. (2023b). Radiology report expert evaluation (ReXVal) dataset.
- Zhai, X., Mustafa, B., Kolesnikov, A., and Beyer, L. (2023). Sigmoid loss for language image pre-training. In *Proceedings of the IEEE/CVF International Conference on Computer Vision*, pages 11975–11986.
- Zhang, H., You, H., Dufter, P., Zhang, B., Chen, C., Chen, H.-Y., Fu, T.-J., Wang, W. Y., Chang, S.-F., Gan, Z., et al. (2024a). Ferret-v2: An improved baseline for referring and grounding with large language models. *arXiv preprint arXiv:2404.07973*.
- Zhang, T., Kishore, V., Wu, F., Weinberger, K. Q., and Artzi, Y. (2020). Bertscore: Evaluating text generation with bert. In *International Conference on Learning Representations*.
- Zhang, X., Zhou, H.-Y., Yang, X., Banerjee, O., Acosta, J. N., Miller, J., Huang, O., and Rajpurkar, P. (2024b). Rexrank: A public leaderboard for ai-powered radiology report generation. *arXiv preprint arXiv:2411.15122*.
- Zheng, L., Chiang, W.-L., Sheng, Y., Li, T., Zhuang, S., Wu, Z., Zhuang, Y., Li, Z., Lin, Z., Xing, E., et al. (2023a). Lmsys-chat-1m: A large-scale real-world llm conversation dataset. *arXiv preprint arXiv:2309.11998*.
- Zheng, L., Chiang, W.-L., Sheng, Y., Zhuang, S., Wu, Z., Zhuang, Y., Lin, Z., Li, Z., Li, D., Xing, E., et al. (2023b). Judging llm-as-a-judge with mt-bench and chatbot arena. *Advances in Neural Information Processing Systems*, 36:46595–46623.

A Appendix

I will provide you with some visual information about a chest X-ray (information that you cannot see) and ask you to create a 5-10 round Q&A conversation between a user and an AI assistant. The assistant should act as if it can visually inspect and interpret the X-ray. Please follow these guidelines:

- The assistant should focus on the visual details that can be reasonably inferred from the X-ray image alone.
- The user’s questions should be diverse and related to the image (appearance, observations, possible abnormalities or bounding box coordinates). Do not hallucinate information outside what I provide you.
- If coordinates for any visual findings are given, ensure they follow the provided format $[x_{min}, y_{min}, x_{max}, y_{max}]$. It should invite the assistant to answer about it, like “Where is [observation] located on the image?”
- The assistant’s answers should be concise, natural, and reflect only what can be seen. Avoid overconfident medical conclusions, and provide cautious, responsible explanations when necessary. You can also provide brief explanations of medical terms (if asked)
- Both questions and answers should feel like a realistic conversation while remaining focused on the image.
- Do not include any extra text or comments outside of the final JSON structure.

Information provided about the X-ray:

- **Radiology report:** There is a right-sided PICC line. There are left-sided chest tubes. There is a small left apical pneumothorax. There is consolidation at the left lung base with prominence of the pulmonary vascular markings throughout the left lung. The right lung appears relatively clear. No pneumothorax on the right side is seen. There is aeration of the atelectasis at the right lung base.
- **List of Abnormalities:** Atelectasis, Consolidation, Pneumothorax, Support Devices
- **View:** AP
- **Gender:** F
- **Selected observations with bounding boxes coordinates:** small left apical pneumothorax: $[0.59, 0.18, 0.77, 0.24]$

Conversation in expected format: [conversation]

Appendix-Figure 1: Prompting LLM to generate conversation data.

Model	Link to Repository
LLaVA-OV	https://huggingface.co/llava-hf/llava-ov-qwen2-7b-si-hf
LLaVA-Med	https://github.com/microsoft/LLaVA-Med
RaDialog	https://huggingface.co/ChantalPellegrini/RaDialog-interactive-radiology-report-generation
CheXagent	https://huggingface.co/StanfordAIMI/CheXagent-2-3b
MAIRA-2	https://huggingface.co/microsoft/maira-2
RadVLM	https://huggingface.co/KrauthammerLab/RadVLM

Appendix-Table 1: Link to repository for each model’s weights

You are an evaluator for a vision-language model. The model answers multi-round questions based on some reference data (referred to as “provided data”). For each round in the conversation, you have:

- User’s question
- Expected answer (if the model had access to the data)
- Generated answer (from the model that does not have direct access to the data, but only to the image)

Your task is to:

- Evaluate each generated answer individually, briefly comparing it to the expected answer in terms of correctness, completeness, and relevance.
- Assign a small “per-question” rating or a short note indicating how close the generated answer is to the expected answer.
- After analyzing all rounds, compute a single final numeric score (0 to 10) that reflects the model’s overall performance across the entire conversation.

Output the final numeric score in the following format only: Overall score: [score]. Do not include any additional text, explanations, or commentary in your final output beyond this line.

Provided Data:

- List of Abnormalities: Edema, Pleural Effusion, Support Devices
- Radiology Report: Port-A-Cath catheter tip is at the level of the right ventricular outflow tract. There is substantial distension of the stomach. What appears to be a ureteral stent is partially imaged. Bilateral pleural effusions, right more than left, are present. Vascular congestion is noted, borderline with mild interstitial pulmonary edema.
- View: AP
- Gender: F
- Selected observations with bounding boxes coordinates: [grounded-phrases]

Conversation to Evaluate:

- **User:** What do you see in this X-ray image?
Expected answer: I see an AP view chest X-ray of a female patient. There appear to be bilateral pleural effusions, more prominent on the right side, and some vascular congestion.
Generated answer: I see a chest X-ray image in the AP view. There are some abnormalities present in the lungs, including an area of increased opacity in the right lung and a small area of increased opacity in the left lung.
- **User:** Can you describe the cardiac silhouette?
Expected answer: (...)

Overall score: [score]

Appendix-Figure 2: Prompting LLM to evaluate conversation inference of a VLM